DesignCon® 2022
WHERE THE CHIP MEETS THE BOARD

Proper Ground Return Via Placement for 40+ Gbps Signaling

Michael Steinberger, MathWorks
msteinbe@mathworks.com

Donald Telian, SiGuys
telian@siguys.com

Michael Tsuk, MathWorks
mtsuk@mathworks.com

Vishwanath Iyer, MathWorks
viyer@mathworks.com

Janakinadh Yanamadala, MathWorks
jyanamad@mathworks.com

Abstract

As signaling rates move beyond 40 Gbps, a proper understanding of Ground Return Vias (GRVs) is imperative. For decades, engineers have placed GRVs next to signal layer transitions based on best practices, with little understanding of relevant quantity and spacing. Place GRVs too far away or pinout a ball-grid array's GRVs incorrectly and a signal via's insertion loss (IL) can drop 40dB. This paper explains the science behind GRVs using practical examples confirmed by mathematics, measurement, and simulation. GRV placement's relationship to data rate and impact on IL, Via Impedance, and Crosstalk are described.

Author's Biographies

Michael Steinberger, Ph.D. Consultant Software Engineer, MathWorks. Michael has over 30 years of experience designing very high-speed electronic circuits. Dr. Steinberger holds a Ph.D. from the University of Southern California and has been awarded 14 patents. He was DesignCon2015's Engineer of the Year. He is currently responsible for the behavioral modeling of mixed analog and digital circuits. Before joining MathWorks, Dr. Steinberger was lead architect for high-speed serial channel analysis at SiSoft.

Donald Telian. Signal Integrity Consultant, SiGuys. Building on over 35 years of SI experience at Intel, Cadence, HP, and others, his recent focus has been on helping customers implement today's highest-speed serial links. Donald is widely known as the SI designer of the PCI bus and the originator of IBIS modeling and has taught SI techniques to thousands of engineers in more than 15 countries. His new book "Signal Integrity, In Practice" brings fresh articulation to the practice of SI for the decades ahead.

Michael Tsuk received his bachelor's, master's, and PhD degrees from the Massachusetts Institute of Technology in 1984, 1986, and 1990, respectively. In 1990, he joined Digital Equipment Corporation, developing their in-house electromagnetic CAD tools. In 2003, he joined ANSYS (formerly Ansoft), focusing on transient simulation of frequency-dependent data. Since 2019, he has been with MathWorks, developing algorithms for signal integrity and radio-frequency applications.

Vishwanath Iyer completed his BE from Univ. of Mumbai in 2001, MS from Utah State University in 2004 and PhD from Worcester Polytechnic Institute in 2010. In 2010, he joined MathWorks as an Application Support Engineer. Since 2013 he has worked on building models of antennas & arrays, fast approximate solvers based on physical optics and integrating the Fast Multipole Method with boundary element method for solving electrically large problems. He is currently a principal software engineer in the RF and Mixed Signal group working on RF PCB Toolbox™ and Antenna Toolbox™.

Janakinadh Yanamadala received his MS and PhD from Worcester Polytechnic Institute in Electrical and Computer Engineering in 2015 and 2016 respectively. In 2016, he joined MathWorks and focuses on development of software for electromagnetics and radio frequency applications.

1 Introduction

While the physical design and manufacture of electronic systems has advanced significantly over the years, changes in dimensions and density in printed circuit boards (PCBs) have been incremental – particularly compared to the exponential increase in integrated circuit (IC) density and system interconnect data rates. Indeed, in the past 30 years IC density has increased 100,000x while PCB density has increased 3x [1, page19]. As such, a challenging convergence of operating frequencies and standard PCB dimensions looms on the horizon. For example, although effort is made to keep 28+ Gbps via stub lengths less than 5 mils, few recognize the surface mount pad stub extending beyond the backside of soldered connector pins is often significantly longer than 5 mils.

Of particular concern and focus in this paper is the placement of ground return vias (GRVs) near signal vias. For decades hardware and layout engineers have added GRVs near signal via layer transitions based on best practices, folklore, and fear with little understanding of where GRVs need to be and why. Mystery and misunderstanding have led to re-routes and wasted PCB real estate. As data rates continue to increase, driving significant spectral content into the 40GHz to 60GHz region, it will become ever more important and difficult to place these GRVs where they will get the job done. The goal of this paper is to describe the role and behavior of GRVs in a way that informs design and layout engineers' intuition and engineering judgement, using practical examples.

Figure 1 shows eight single ended signals under a 1 mm pitch ball-grid array with equivalent ~100 mil vias to the route layer shown, next to measured data for the same. Each of the eight signal vias is immediately surrounded by four GRVs. However the pattern of the GRVs varies, depending on where each signal falls within an alternating 2 mm array of GRVs. The GRVs in the sites labeled "diamond" are closer to their associated signal via (1 mm) than the GRVs in the sites labeled "square" are to their associated signal via (1.4 mm). Measured data (at right) reveals the "square" signal's insertion loss (IL) decreases to -40 dB at 40 GHz while the "diamond" signal's IL continues to decrease linearly. How is it possible, simply due to ground via placement, that 99% of the signal is lost for half of the signals while IL for the other half is well-behaved? Furthermore, how can a tiny 100-mil via structure within the same dielectric material exhibit more loss than fifteen inches of trace? This paper will demonstrate the answers lie in understanding the interactions of the via's return currents.

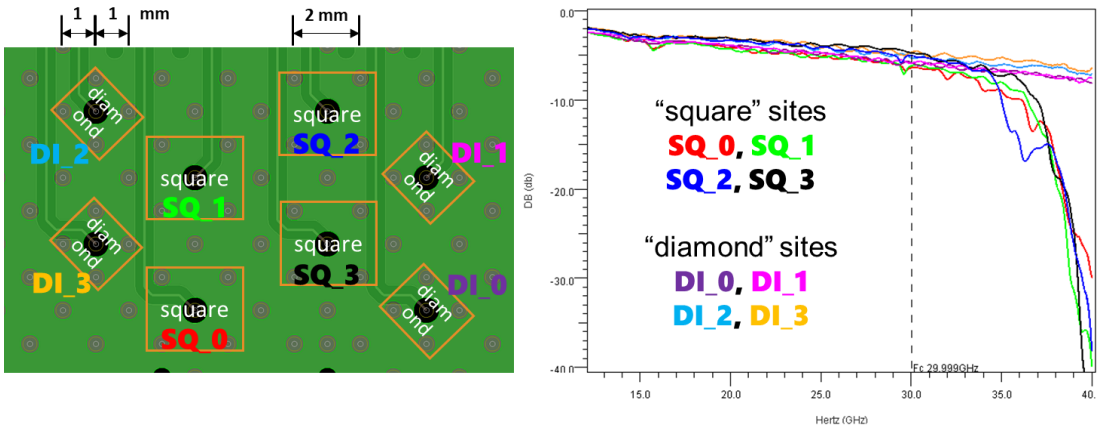

Figure 1: PCB test structure and resulting signal IL

This paper will demonstrate what happens when GRVs are too distant for the data rate at hand. When the distance from the signal via to the GRVs in Figure 1 becomes greater than approximately a quarter wavelength, the structure resonates with a relatively high Q. It is in effect a microwave filter. To help avoid the excessive IL shown in Figure 1, this paper will define a Gap-Rate Distance (GRD) metric that can be easily applied to GRV placement in a PCB layout.

We will use three metrics in both simulation and measurement to gauge the efficacy of passive interconnects as influenced by GRV placement: IL, time domain reflectometry (TDR), and crosstalk. While IL currently gets the most attention because it both reduces the signal amplitude and is a major source of intersymbol interference, SerDes equalization schemes and lower-loss materials have been effective at mitigating IL effects. However, as the authors have been asserting for a long time [2, 3, 4], transmission path discontinuities, as measured by TDR, are every bit as serious a source of intersymbol interference, and significantly more difficult to equalize. Indeed, as increasing miniaturization impacts electronic products, discontinuities are becoming the primary cause of link failure [1, Chapter 4].

Measured TDR in Figure 2 demonstrate that the GRV placements that affect IL in Figure 1 also cause unexpected discontinuities in the transmission path. For ~15 ps, a perturbation relevant to current data rates, the signal via impedance is consistently five ohms higher for the "square" sites than the "diamond" sites. Although one such increase in via impedance might not be a serious problem, multiple irregular vias along a transmission path can cause serious impairments.

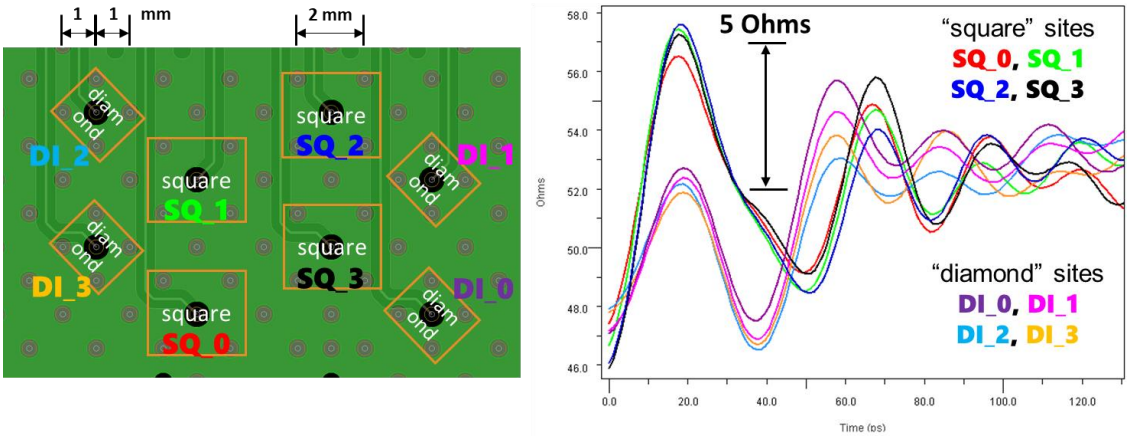

Figure 2: Measured TDR for eight test signal vias

Finally, as the measured data and model results in this paper will show, crosstalk is going to become a serious impairment as data rates increase. As shown in Figure 3, measurements demonstrate that at higher frequencies crosstalk between the "square" sites (gold) is higher than the crosstalk between a "square" site and a "diamond" site (blue), which in turn is higher than crosstalk between two "diamond" sites (black). Crosstalk increases rapidly with frequency and is primarily a function of GRV configuration. Note also from the layout that the signal vias are not at all "close" to each other compared to crosstalk dimensions normally considered, indicating some effect beyond capacitive coupling is at work, as will be demonstrated. Although differential transmission improves the situation somewhat, a similar phenomenon occurs for that case as well.

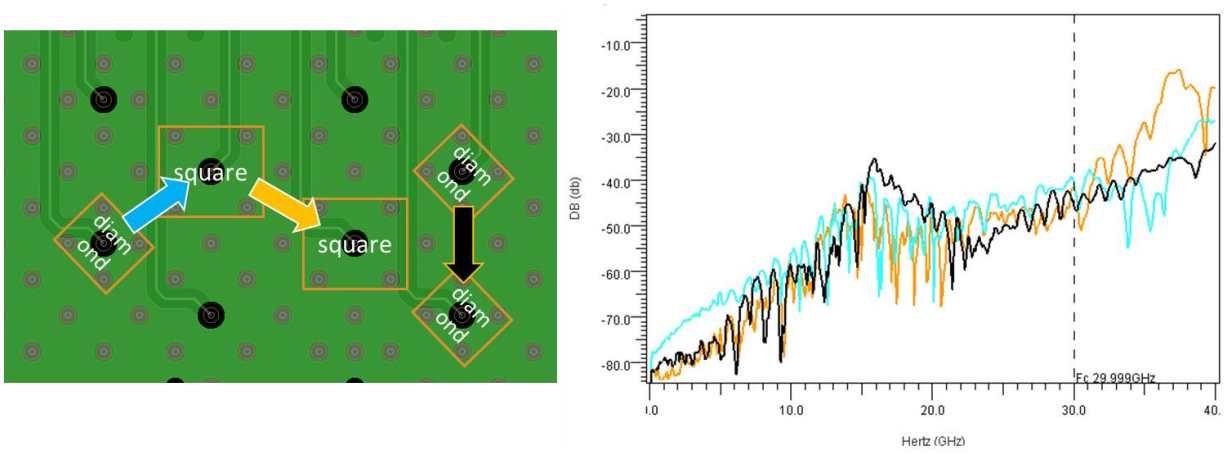

Figure 3: Measured crosstalk for signal vias

This paper is a natural extension of the authors' compute-efficient and structure-based approach to via modeling [5, 6, 8] to include effects of higher frequencies. While many current applications use differential transmission, this paper will concentrate on single-ended transmission because the role of the GRV is simpler to illustrate and comprehend. However, we will briefly address differential transmission in section 7.1 near the end of the paper.

2 Technical Overview

The primary purpose of this paper is to integrate known concepts [7, 8, 9] in a way that informs the engineering judgement of circuit board and electronic package designers for high-data-rate applications. We will therefore build our description and circuit equations on a visualization of the voltages and currents in the structures to be analyzed.

The first step is to visualize the voltages and currents in a via carrying a signal. To do this, we break the via into via cells, where each via cell describes the behavior in a single dielectric layer ("layer") bounded top and bottom by conducting planes ("return planes"). While the signal flows along the via barrel in the same way that it would in a coaxial transmission line, the return current must flow outward along the return planes in the form of a radial TEM wave - that is, a wave that flows from a center outward in all directions along the return planes and dielectric layer like ripples in a pond. The only way the return current can get across the via cell is either through the impedance of the radial TEM wave itself or else through transportation by the radial TEM wave to other structures such as GRVs that will conduct the return current across the dielectric.

Supposing that some of the return current has been conducted to a GRV and along the via barrel of the GRV to the other side of the dielectric, the only way it can get conducted back to the signal via is by another radial TEM wave. This radial TEM wave will interact directly with the via cell and will also interact with other structures in the layer, such as other via cells or GRVs.

Thus, there will be a number of radial TEM waves flowing throughout the dielectric layer and interacting with other structures in the layer. The waves flow at a finite velocity and the structures are separated by finite distances, so the interactions within the return layer will be frequency dependent and can get somewhat complicated.

Following the visual description of the physical phenomena, our analysis will start with the interaction between a single via cell and a single GRV. There are only two radial TEM waves involved, and we will show how they combine to produce a frequency-dependent impedance in the return path of the via cell. We will then generalize these equations into a relatively straightforward matrix equation that can be applied directly to the entire layer and all the structures in it. The radial TEM waves in the return path are also the primary means of crosstalk coupling between vias, and this behavior is an integral part of the matrix equation.

In the computational section that applies the general matrix equation to more complex structures such as combinations of multiple via cells and multiple GRVs, we will discover that when multiple GRVs surround a single via cell, their waves can interact constructively, creating a resonant cavity that can cause the behavior of the return path to change abruptly for frequencies near the resonant frequency. We will study how these resonances affect IL, path discontinuities and crosstalk observed in the structures under study, and we will supply a Gap-Rate Distance (GRD) metric that can make it more convenient to determine when a given layout might exhibit some of these behaviors.

This paper will conclude with a brief description of several ongoing efforts to extend the range of via structures to which this type of analysis can be applied.

3 Via Cell

For the purposes of this paper, a "via cell" is a subsection of a via that transitions from one conducting plane, through one or more dielectric layers (possibly containing signal routing), to another conducting plane. Figure 4 illustrates a case in which there is one via, four conducting planes, and three dielectric layers. There are three via cells in this figure, and the via cell indicated by the labeling is the via cell connecting the second and third conducting planes.

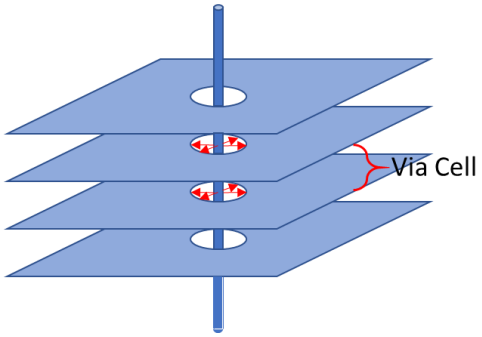

Figure 4: A single via cell in a layered structure

It is expected that the via cell will be analyzed as part of an electromagnetic solution for the dielectric between two conducting layers and, as described for example in [8], the layer solutions will be combined to produce a result for the complete PCB or package structure. Similar to other solutions, our method for combining the layers is to calculate a generalized circuit ("ABCD") matrix for each layer and cascade the ABCD matrices to produce an ABCD matrix for the entire structure. In our particular method, the ABCD matrices are extended to include S parameter ports, each of which is connected to a specific physical location on a specific layer and then

propagated to be represented in the end-to-end ABCD matrix. An output S parameter matrix is then calculated from the end-to-end ABCD matrix.

Also, for the sake of simplicity and clarity, this paper assumes that all via cells are single-ended and circularly symmetric. That is, each consists of a single cylindrical via barrel at the center of a circular antipad. Many other geometries are of course possible, including differential vias and a variety of antipad shapes. However, for the purposes of the return path analysis presented here, each of these can be transformed into an equivalent single-ended, circularly symmetric via through an appropriate choice of via barrel radius and antipad radius.

3.1 Near Fields

This section describes the electric fields, magnetic fields, and current flow in the immediate vicinity of the barrel and antipad of a via cell. These concepts drive the definition of the circuit model of the via cell and provide a set of boundary conditions for the return path fields.

For the purposes of this analysis, it is assumed that the via has been dimensioned to support only TEM transmission at the highest frequency of interest. Even at 40 GHz, almost all designs satisfy this assumption with significant margin. Under these conditions, the electric field inside the via cell is circularly symmetric, with a cross section similar to that illustrated in Figure 5.

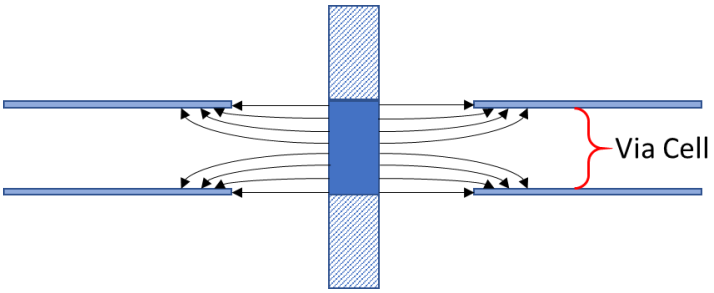

Figure 5: Electric fields in a typical via cell

The measured data we have analyzed indicates that the impedance of a via is typically between 5% and 10% higher than that of a coaxial transmission line with the same dimensions, and our static electromagnetic analysis matches the measured data well within experimental error. The electric fields from the via barrel do extend past the edge of the antipad by perhaps as much as 20% of the antipad radius but not significantly further.

The magnetic field within a via cell is circularly symmetric as well, exactly like the magnetic field in a coaxial transmission line. Figure 6 illustrates the classic evaluation of the magnetic field using Maxwell's fourth equation.

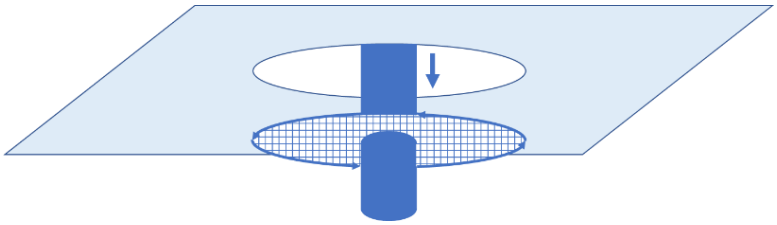

Figure 6: Evaluation of the magnetic field generated by the via barrel

A loop is defined around the conductor and a surface is defined inside the loop. The magnetic field integrated along the loop is equal to the integral of the current density crossing the surface plus the time derivative of the electric field crossing the surface, as described in Maxwell's fourth equation (equation (1) below). The so-called "right-hand rule" is used to relate the sign of the loop integral to the sign of the surface integral, in that if the thumb of the right hand points in the direction of surface integration, the curled fingers point in the direction of loop integration.

In Figure 6, the current crossing the surface is the current flowing along the via barrel. In many cases, including this one, the time derivative of the electric field crossing the surface can be neglected, in this case because, as illustrated in Figure 5, the electric field is essentially parallel to the surface and therefore has no significant component crossing the surface. Thus, in Figure 6 the magnetic field is proportional to the current in the via barrel.

Expressed in its integral form using the variables that will be used in this paper, Maxwell's fourth equation is [7]

$$\oint H \cdot dl = \iint_S J \cdot dS + \frac{\partial}{\partial t} \iint_S \epsilon E \cdot dS \tag{1}$$

where H is the magnetic field in amperes per meter, J is the current density in amperes per square meter, ϵ is the dielectric constant in farads per meter, and E is the electric field in volts per meter.

This method can also be used in other ways to provide direct insight into the fields and currents in the via cell. In Figure 7, the magnetic loop has been expanded to be larger than the antipad, and moved inside the conducting plane above the via cell in order to measure the total current entering the via cell. Because the magnetic loop now surrounds the antipad, the current crossing the edge of the antipad is crossing the integration surface along with the via barrel current.

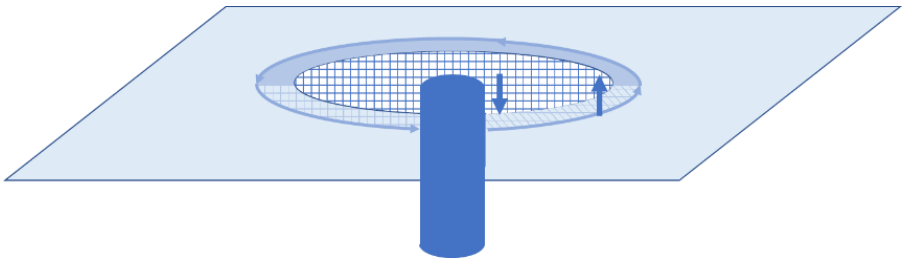

Figure 7: Magnetic loop placed inside conducting layer to measure the total current entering the via cell

At frequencies for which the conducting plane is many skin depths thick (typically frequencies greater than 100 MHz), the magnetic field inside the conducting plane is essentially zero, and so the loop integral is zero. Therefore, the total current crossing the surface is zero. As illustrated in Figure 8, the total current crossing the edge of the antipad is exactly equal in magnitude and opposite in direction to the current flowing in the via barrel.

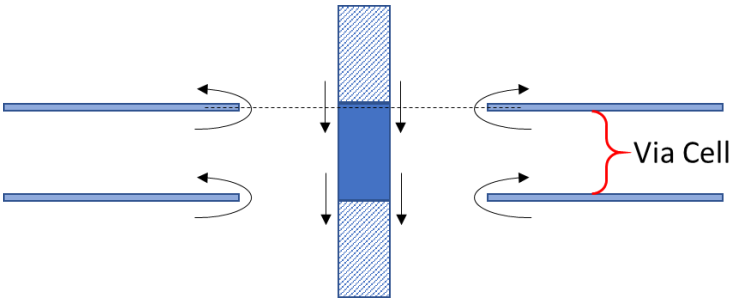

Figure 8: Current flow into and out of the via cell

This result can be checked by creating yet another loop and surface. Suppose a magnetic loop below the conducting plane is broken and connected to a similar magnetic loop inside the conducting plane, as illustrated in Figure 9. Then the total loop goes around the loop below the conducting plane, up into the conducting plane, around the loop inside the conducting plane, and back down to reconnect with the loop below the conducting plane. The cylindrical surface that is created then measures the current flowing on the surface of the conducting plane. The loop integral for the combined loop is the same as for the loop integral associated with Figure 6, and so the total currents are the same. Using the right-hand rule, the directions work out correctly as well.

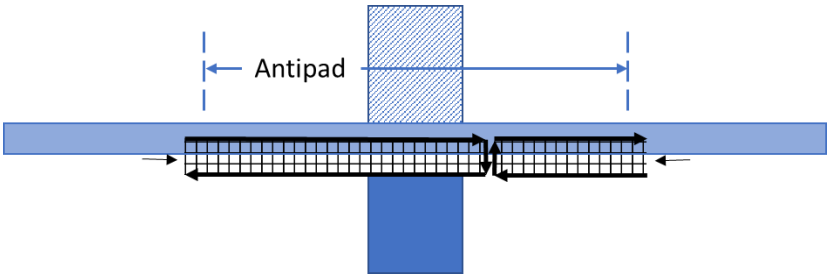

Figure 9: Magnetic loop and surface to measure the current flowing in the conducting layer above the via cell.

3.2 Return Path Fields

As described in section 9.3 of [7], the conducting planes around the via cell support a radial TEM wave that is centered on the via cell and flows parallel to the conducting planes in all directions from the antipad of the via cell. Radial TEM waves will also be reflected from each GRV, from current induced in other via cells, and from the edges of the board, producing an effect very similar to the waves produced when a pebble is dropped into a pond.

The electric field of the radial TEM wave is uniform in the direction perpendicular to the conducting planes ("z" direction) and the magnetic field is parallel to the conducting planes and circularly symmetric. The equations for this wave are

$$E_Z = AH_0^{(2)}(kr) \tag{2}$$

$$H_\phi = \frac{j}{\eta} AH_1^{(2)}(kr) \tag{3}$$

where $H_0^{(2)}(v) = J_0(v) - jN_0(v)$ is a zero order Hankel function of the second kind, composed of Bessel functions of the first and second kinds; similarly, $H_1^{(2)}(v) = J_1(v) - jN_1(v)$ is a first-order Hankel function of the second kind; $\eta = \sqrt{\frac{\mu}{\epsilon}}$ is the impedance of the dielectric; $k = \omega\sqrt{\mu\epsilon} = \frac{2\pi}{\lambda}$ is the propagation constant; and r is the radius from the center of the mode.

Note that as described in [8] and based on the classic paper by Djordjevic et al. [10], the wave propagation velocity will be accurate only if the dielectric constant is a complex number that reflects the dielectric loss tangent as well as the relative dielectric constant and the dielectric constant of free space. The simplified equation for the relative dielectric constant given in [8] is

$$\epsilon_r(\omega) = \epsilon_\infty + \frac{2Re\big(\epsilon_r(\omega_0)\big)tan\delta}{\pi}\ln\left(\frac{\omega_2 + j\omega}{\omega_1 + j\omega}\right) \tag{4}$$

where ϵ_∞ is the dielectric constant at extremely high frequencies, ω_0 is a radial frequency for which the relative dielectric constant $\epsilon_r(\omega_0)$ is specified, $tan\delta$ is an essentially constant dielectric loss tangent, ω_1 is a relatively low radial frequency limit (typically 10 kHz), and ω_2 is a relatively high radial frequency (typically 1 THz).

At the antipads, the voltage induced between the conducting planes is

$$V = -E_z d \tag{5}$$

where d is the distance between the conducting planes. The current flowing into the upper antipad and out from the lower antipad is

$$I = 2\pi r H_\phi \tag{6}$$

Although section 7 addresses higher order modes, this so-called "zero order" mode has proven to be sufficient to produce calculated results that match measured data.

3.3 Circuit Model

The equivalent circuit for the via cell is shown in Figure 10. So long as the dielectric layer thickness is less than or equal to a tenth of a wavelength at the maximum frequency of interest, the portion of the via cell inside the antipad can be very accurately modeled as a single pi section lumped circuit. This assumption is valid for almost all applications. For higher frequencies or greater layer thicknesses, the via cell should be modeled using a more detailed lumped model or a distributed model.

The return impedance, shown as Z_R in Figure 10, represents the impedance of the return path through the antipad currents. Because the return path can easily be several wavelengths long at a frequency of interest, it must be modeled using a distributed model. This return impedance is the primary subject of this paper.

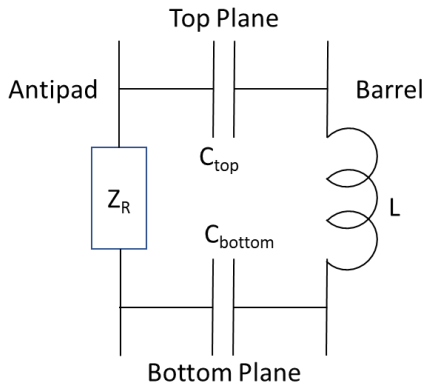

Figure 10: Circuit model for via cell

The barrel inductance models the effect of the magnetic field inside the antipads, but not any of the magnetic fields that are outside the antipads and therefore part of the return path. Considering the speed of light in the dielectric ($1/\sqrt{\mu\epsilon}$) and the characteristic impedance of a coaxial transmission line $\left(1/2\pi\sqrt{\mu/\epsilon}\, ln(R/r)\right)$, and given a dielectric thickness d, via barrel radius r_b, and antipad radius r_a, the barrel inductance is

$$L_{barrel} = \frac{\mu d}{2\pi} ln\left(\frac{r_a}{r_b}\right) \tag{7}$$

Although the via barrel capacitance can be roughly estimated using a similar application of coaxial transmission line equations, such an approximation usually underestimates the via impedance by 5% to 10%, as mentioned in section 3.1. The barrel capacitance can be calculated much more accurately by any of a number of numerical methods. In our experience a static field calculation has proven to match measured data consistently, within experimental error for this lumped capacitance.

The remainder of the via cell circuit response, and especially any inductance due to magnetic fields outside the antipad, is determined by the return path impedance. The return path, in turn, is a combination of the radial TEM wave launched from the edge of the antipad plus the effect of any GRVs nearby. Section 3.4 presents the analysis of the impedance in the absence of GRVs, section 4 adds the effect of a single GRV, and section 5 includes the effect of multiple GRVs.

Note that with the rare exception of via cells that are so close together that they couple capacitively, the return path is also the primary mechanism for crosstalk coupling. The wave from each via cell is not completely terminated by the nearby GRVs, but rather propagates throughout the rest of the layer, inducing voltages across the return impedances of the other via cells in the layer. The computational results will demonstrate that, at least for single-ended vias, crosstalk coupling due to the return path is not a particularly sensitive function of distance.

3.4 Layer Boundary Conditions

The modeling in this paper will use absorbing boundary conditions as presented, for example, in [9]. It is also possible to model open circuit boundary conditions at the edge of either a square or circular circuit board. However, those refinements don't appear necessary for the cases studied in this paper.

The voltage drop at the edge of the antipad (radius r_a) is given by equation (5) and the current is given by equation (6). The return path impedance is then

$$Z_R = \frac{V}{I} = \frac{-AdH_0^{(2)}(kr_a)}{2\pi r_a A \frac{j}{\eta} H_1^{(2)}(kr_a)} = \frac{jd\eta}{2\pi r} \frac{H_0^{(2)}(kr_a)}{H_1^{(2)}(kr_a)} \tag{8}$$

Figure 11 is a plot of the real and imaginary parts of the return impedance with absorbing boundary conditions, for the dimensions of the via cell for the measured data used in this paper.

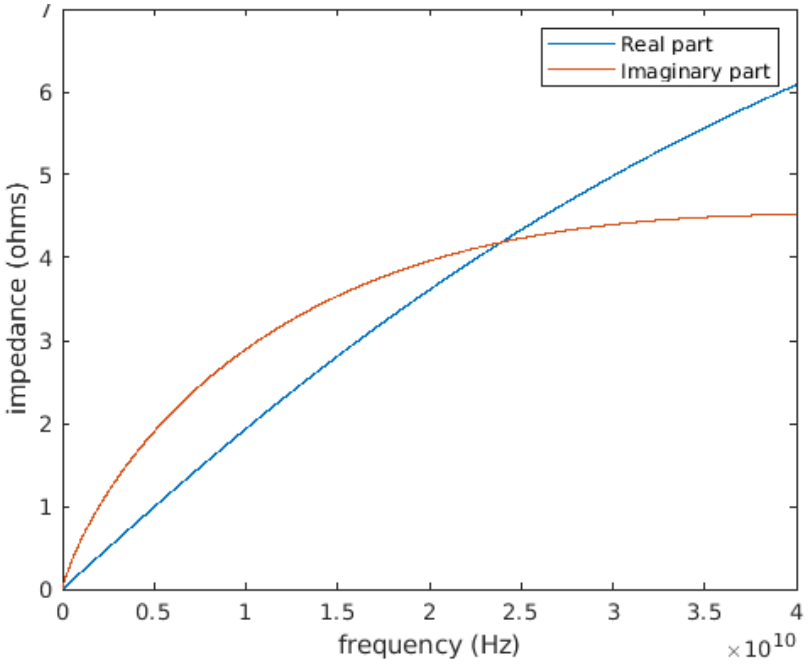

Figure 11: Return impedance with absorbing boundary conditions

There are several interesting observations that can be made about the data in Figure 11.

- The return impedance tends toward zero at low frequencies and increases continuously with frequency.
- The real part of the impedance is comparable to the imaginary part.
- The imaginary part of the impedance indicates an inductance, consistent with our expectation in section 3.3, of an inductive component from the return impedance.

4 Ground Return Via

A GRV is formed when a via barrel is shorted directly to the conducting planes both above and below a dielectric layer. It acts as a nearly ideal short-circuit reflector, producing an outgoing radial TEM wave in response to the total voltage applied by the other waves in the layer, in such a way as to cancel the incoming wave and reduce the voltage at the GRV to essentially zero.

When the GRV is close enough to a via cell, the reflected wave from the GRV propagates back to the via cell in time to partially cancel the voltage from that via cell's outgoing return path wave, thus reducing the via cell's return path voltage and therefore its return path impedance. However, if the via cell's outgoing wave gets delayed by ninety degrees (one quarter wavelength) on its way to the GRV, and then the wave from the GRV back to the via cell gets delayed by another ninety degrees, then the wave from the GRV will be too late to subtract from the via cell's return path voltage, and may actually add to it. *This basic phenomenon is the fundamental topic of this paper.*

The basic phenomenon is enhanced when there are multiple GRVs near the same via cell. The wave reflected from one GRV not only affects the via cell return voltage directly, but propagates past the via cell to be reflected by the other GRVs. This can set up a constructive interference pattern that significantly increases the net effect of the GRVs. This effect is demonstrated clearly by the results presented in section 6.

This section presents the derivation of the response for a single GRV and demonstrates how a single GRV will interact with a single via cell. This analysis will then be extended in section 5 to demonstrate the application to more complex configurations.

4.1 GRV Reflection Coefficient

Figure 12 illustrates the voltages and currents associated with a GRV. The GRV responds to a total incoming voltage wave V_{in}, producing an outgoing radial TEM voltage wave V_{out}. There is a current I associated with this outgoing wave, and this current flows through the via barrel of the GRV. The via barrel has a small internal impedance Z_{int}, and the voltage drop across this impedance must match the sum of V_{in} and V_{out}. In practice, Z_{int} is negligibly small, so that the practical result is $V_{out} \approx -V_{in}$. This section will present a more detailed analysis in order to enable greater insight into the underlying physical processes.

In Figure 12, the current in the via barrel is the current for the outgoing radial TEM wave for which the voltage is V_{out}, and this current therefore flows outward at the top of the via barrel and in at the bottom.

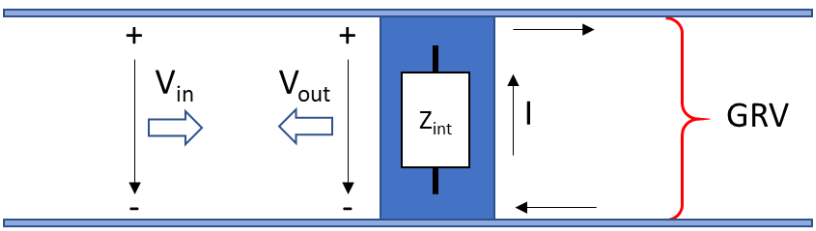

Figure 12: GRV voltages and currents

The circuit equation is

$$V_{in} + V_{out} = -IZ_{int} \tag{9}$$

The GRV has an external wave impedance defined as

$$Z_{ext} \equiv \frac{V_{out}}{I} \tag{10}$$

Combining these two equations by substituting $I = {V_{out}}/{Z_{ext}}$ in equation (9) and solving for V_{out},

$$V_{out} = -V_{in} \frac{Z_{ext}}{Z_{ext} + Z_{int}} \tag{11}$$

All that remains is to define equations for Z_{ext} and Z_{int}. Define the following variables:

r_{b1}	GRV barrel radius
r_{b0}	GRV finished hole radius
σ	GRV barrel conductivity

Then, essentially the same as in equation (8), equations (2), (3), (5), and (6) can be combined to produce

$$Z_{ext} = \frac{jd\eta}{2\pi r} \frac{H_0^{(2)}(kr_{b1})}{H_1^{(2)}(kr_{b1})} \tag{12}$$

The derivation of Z_{int} requires a detailed understanding of waves flowing in conducting surfaces, such as the description found in section 4.5 of [7] of currents flowing in round wires. Especially for frequencies at which the skin depth is much less than the radius of the wire (or via barrel), the skin impedance consists of an inductive component and a resistive component of equal magnitude.

$$Z_{int} \approx (1 + j) \frac{d}{2\pi r_{b1}} \sqrt{\frac{\omega\mu}{2\sigma}} \tag{13}$$

The equations for Z_{int} could be made even more precise at high frequencies by accounting for the very thin layer of lossy dielectric on the surface of the via barrel [11, 12], formerly referred to as the "surface roughness" effect. However, that level of precision is not required for this application.

Figure 13 is a logarithmic plot of both the real and imaginary parts of Z_{ext} and Z_{int} for the GRVs used for the measured data presented in this paper. (As noted above, the real and imaginary parts of Z_{int} are nearly equal.) In this case, Z_{ext} is approximately 10^3 larger than Z_{int}, justifying the assertion that the GRV is a nearly ideal short-circuit reflector.

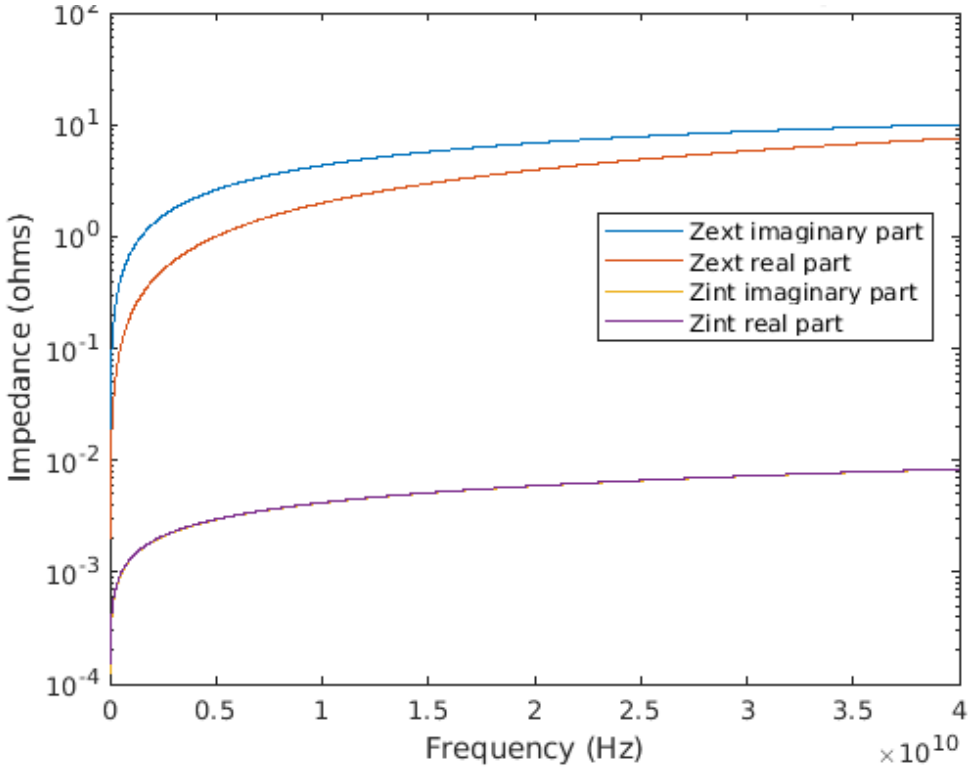

Figure 13: GRV external and internal impedances vs. frequency

4.2 Via Cell – GRV Interaction

The return path voltage for a via cell is the sum of voltage contributions from every electromagnetic mode in the layer. This, of course, includes the voltage from the via cell's outgoing return path wave, but also includes a contribution from every mode from every other via cell, GRV, or reflecting edge in the layer. This subsection will consider voltages from only a single via cell and a single GRV; however, this is only a simple demonstration of the more general case.

The return path current for a via cell is determined directly by the via cell's zero-order outgoing radial TEM wave (or waves). As considered in detail in section 3.1, the return path current can be determined by integrating the magnetic field around a loop that surrounds the via cell.

The return path impedance Z_R shown in Figure 10 is therefore the sum of all of the mode voltages at the edge of the antipad divided by the return current coming from inside the via cell. This impedance then becomes one circuit element in the larger circuit to be solved.

Consider the case of a via cell with a GRV the center of which is located at a radius R from the center of the via cell. Let V_{out1} be the outgoing wave voltage for the via cell, and let V_{out2} be the outgoing wave voltage for the GRV. Similarly, let V_{in1} and V_{in2} be the total voltages due to other waves at the via cell and the GRV, respectively.

Then the voltage of the wave impinging on the GRV will be the voltage generated by the via cell outgoing wave at the GRV:

$$V_{in2} = \frac{H_0^{(2)}(kR)}{H_0^{(2)}(kr_a)} V_{out1} \equiv P_{12} V_{out1} \tag{14}$$

The voltage of the reflected wave just outside the via barrel of the GRV will be a nearly perfect reflection (reflection coefficient $\Gamma_2 \approx -1$)

$$V_{out2} = \Gamma_2 V_{in2} \tag{15}$$

This wave will propagate back to the via cell to apply a voltage at the via antipad (averaged around the antipad, therefore evaluated at the center-to-center distance, R)

$$V_{in1} = \frac{H_0^{(2)}(kR)}{H_0^{(2)}(kr_{b1})} V_{out2} \equiv P_{21} V_{out2} \tag{16}$$

The total voltage at the antipad (radius r_a) will be the voltage originally produced by the via cell minus the voltage from the GRV

$$V_{total} = V_{out1} + V_{in1} = (1 + P_{21}\Gamma_2 P_{12}) V_{out1} \tag{17}$$

Applying equation (8), the return impedance $Z_{R(1GRV)}$ will be

$$Z_{R(1GRV)} = (1 + P_{21}\Gamma_2 P_{12}) Z_R \approx \frac{jd\eta}{2\pi r_a} \frac{H_0^{(2)}(kr_a) - \frac{\left(H_0^{(2)}(kR)\right)^2}{H_0^{(2)}(kr_{b1})}}{H_1^{(2)}(kr_a)} \tag{18}$$

5 General Form for Return Path Equations

Many return path analyses involve multiple via cells and an even larger number of GRVs in a single dielectric layer. Analyses involving multiple via cells usually also require an estimate of crosstalk as well as reflection coefficient. Therefore, the analysis should be organized in a general form that addresses all the requirements.

Consider an analysis involving n via cells and $m \geq n$ radial TEM waves. There will be one outgoing zero-order radial TEM wave centered in each via cell and another one centered in each GRV. There can also be higher-order modes associated with the via cells and modes associated with edge reflections. Define

- $\mathcal{I}$: An $n \times 1$ vector of via cell return currents
- $\mathcal{V}_{out}$: An $m \times 1$ vector of outgoing wave voltages, one for each wave, as measured at the antipads of the via cells and the via barrels of the GRVs
- $\mathcal{V}_{in}$: An $m \times 1$ vector of incoming wave voltages, one for each wave, as measured at the antipads of the via cells and the via barrels of the GRVs

- $\mathcal{V}_{return}$: An $m \times 1$ vector containing the total return path voltages, as measured at the antipads of the via cells and the via barrels of the GRVs

Then, analogous to equation (14), the wave propagation can be expressed as

$$\mathcal{V}_{in} = P\mathcal{V}_{out} \tag{19}$$

where P is an $m \times m$ matrix of propagation constants. For zero-order modes, the entries in this matrix are

$$P(j,k) = \frac{H_0^{(2)}(kR_{jk})}{H_0^{(2)}(kr_k)} \quad j \neq k, \qquad = 0 \; otherwise \tag{20}$$

with R_{jk} the center-to-center distance between waves and r_k the radius at which the outgoing wave voltage is defined.

The entries in $\mathcal{V}_{out}$ are defined either as being driven by via cell return current or as being the reflection of incoming waves. The general equation is a combination of equation (8) for the via cells and equation (11) for the GRVs:

$$\mathcal{V}_{out} = Z\mathcal{I} + \Gamma\mathcal{V}_{in} \tag{21}$$

where Z is an $m \times n$ matrix of return path impedances and Γ is an $m \times m$ matrix of propagation constants. If the via cell waves are in rows 1 through *n* of $\mathcal{V}_{out}$, then the entries of Z and Γ are

$$Z(j,j) = \frac{jd\eta}{2\pi r_j} \frac{H_0^{(2)}(kr_j)}{H_1^{(2)}(kr_j)} \quad j \leq n, \qquad = 0 \; otherwise \tag{22}$$

$$\Gamma(j,j) = -1 \quad j > n, \qquad = 0 \; otherwise \tag{23}$$

The solution to equations (19) and (21) is

$$\mathcal{V}_{out} = (I - \Gamma P)^{-1} Z\mathcal{I} \tag{24}$$

The total return voltage is then

$$\mathcal{V}_{return} = \mathcal{V}_{out} + \mathcal{V}_{in} = (I + P)(I - \Gamma P)^{-1} Z\mathcal{I} \equiv Z_{return}\mathcal{I} \tag{25}$$

Note that Z_{return} is an impedance matrix that contains both return impedance and crosstalk terms. The diagonal elements of the matrix are the return impedances created in the individual via cells, while the off-diagonal terms describe the crosstalk between via cells and the coupling between the via cell return currents and the residual voltages at the GRVs.

6 Computational Results

We applied equation (25) to the layout shown in Figure 1, eventually including more via cells and GRVs, stacked into a full PCB layer stackup. We did not include all of the features on all of the layers, and some of those variations were significant. Nonetheless, modeling the PCB as numerous layered via cells, is a decent approximation of the design that was measured, and hence a qualitative comparison can be made to the measured data in Figure 1 through Figure 3.

Considerable insight will be gained by building the model element by element and observing how the interaction between GRVs affects the behavior of the structure.

6.1 Insertion Loss (IL)

Figure 14 shows the real and imaginary parts of the return path impedance as the number of GRVs closest to a "square" test site is varied between one and four. While the imaginary part shows a fairly consistent inductance, at least up to 20 GHz, the real part of the return path impedance varies considerably. For one GRV, the real part of the impedance is a modest variation of the absorbing boundary layer impedance shown in Figure 11, while for four GRVs, the real part is very close to zero up to about 25 GHz, but then increases abruptly to a peak around 36 GHz.

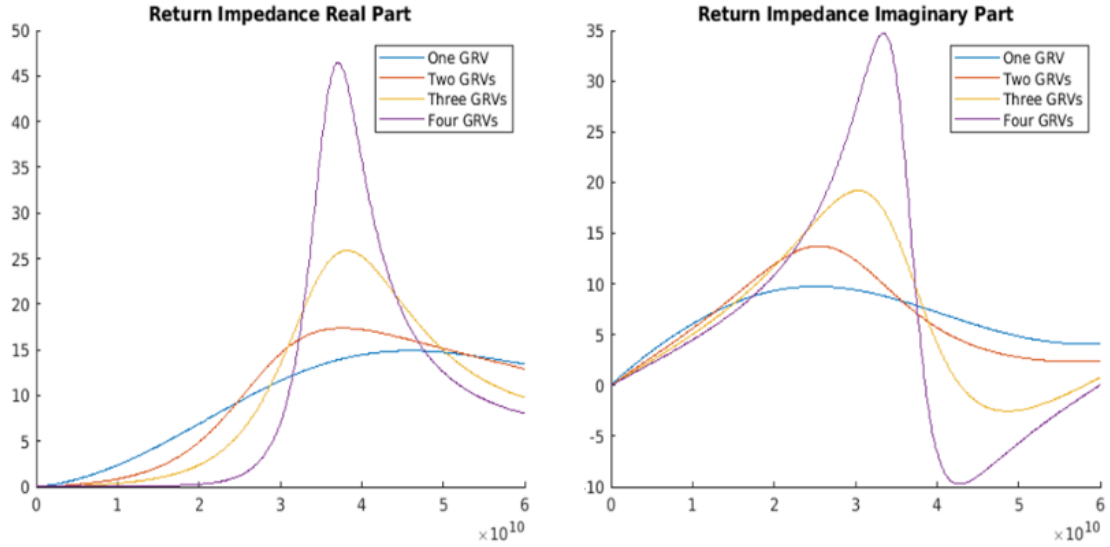

Figure 14: Return path impedance as a function of the number of GRVs

The variation of return impedance in Figure 14 is due to the constructive interference of the radial TEM waves reflected from the GRVs, leading to a resonance around 36 GHz. As the configuration of the GRVs comes closer to enclosing the signal via, the Q of this resonance increases significantly. The GRVs form a Faraday cage, and the holes in this Faraday cage get smaller when there are more bars in the cage, thus improving the shielding.

Figure 15 is a plot of the single-layer IL for one through four GRVs at a "square" test site, as well as for that test site when 8 GRVs for the structure shown in Figure 1 are included. As the number of GRVs is increased the onset frequency of the resonant behavior increases. At the center frequency of the resonant response, the maximum distance between GRVs is seen to be

slightly more than a half wavelength. It appears that the resonant mode is something between the resonant mode that would exist for a solid walled square cavity with corners at the GRVs and the resonant mode that would exist for a solid cylindrical shield connecting the GRVs.

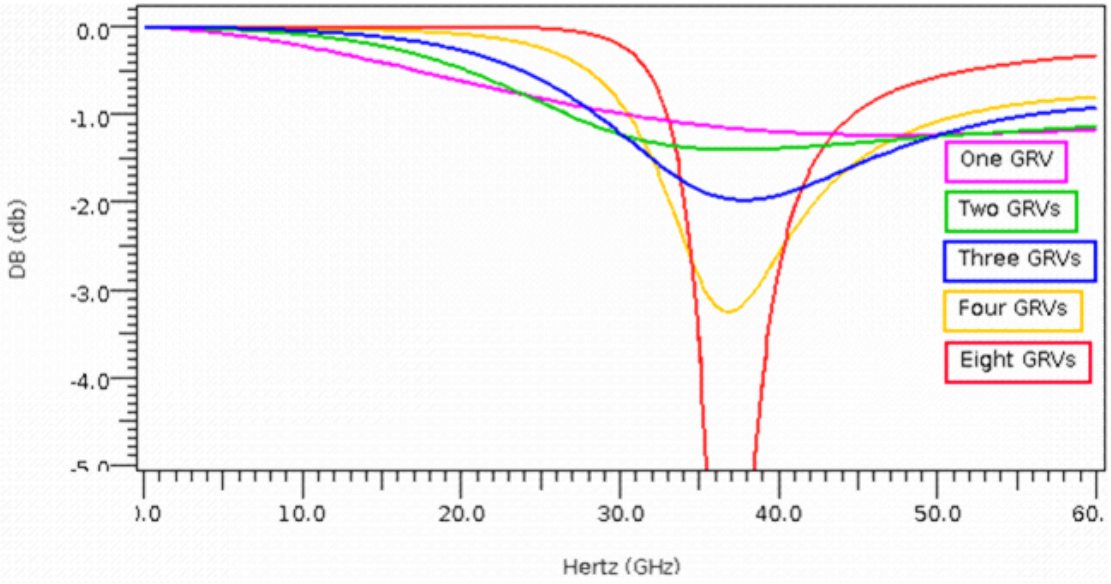

Figure 15: Single-ended IL as a function of the number of GRVs, one layer

Note again that Figure 15 models *only one via cell layer*, and yet the rapid IL decrease near the ¼ wavelength frequency of the GRVs is seen even in this small structure. We have found that, when stacking additional via cells, the phase shift between layers is enough to compound the resonant response increasing the IL magnitude towards that seen in Figure 1, making the via start to resemble a multi-cavity filter rather than a series connection of lumped circuit elements. Obviously, past the onset of the resonant response the vias are not likely to be suitable for any practical application.

6.2 Critical Wavelength and Gap-Rate Distance

Considering the previous section's demonstration of how vias with insufficient GRV structures become very high-loss components, this section develops metrics to help avoid such structures in practice. We first define a Critical-Wavelength (*CW*) metric for GRV to signal via (SV) center-to-center distance d, operating frequency f, and relative dielectric constant ϵ_r and c the speed of light in a vacuum:

$$CW = \frac{df\sqrt{\epsilon_r}}{c} \tag{26}$$

Figure 16 is a nomogram for this metric, supporting ϵ_r values of 2.0, 3.0, and 4.0. The GRV gap distance is chosen on the left-hand side of the nomogram, and the frequency is chosen on the right-hand side. A straight line drawn between these two points will intersect the CW value on the line in the middle of the nomogram. Figure 16 further demonstrates the calculation of the CW for the 1.4 mm gap of a "square" test site at 30 GHz and a dielectric constant of 3.0. The dashed line intersects the line in the middle at a CW value of 0.25, indicating a quarter wave at that frequency.

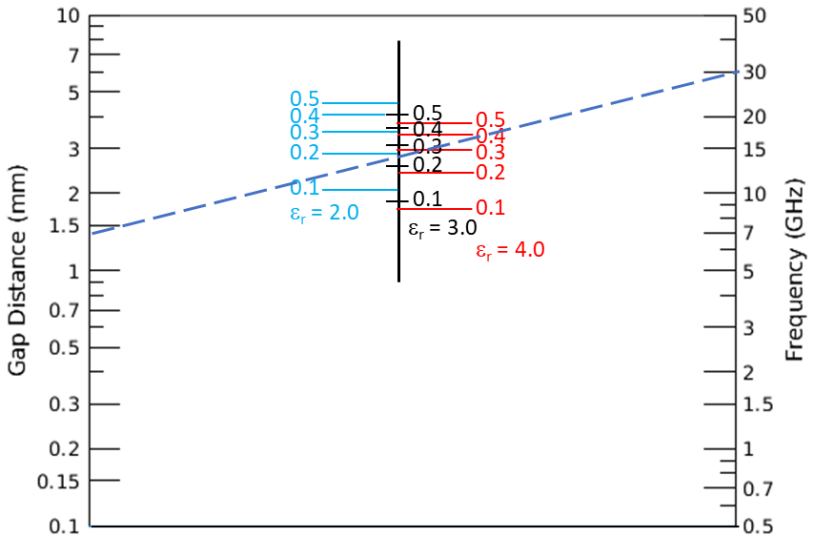

Figure 16: CW nomogram with demonstration at 1.4mm, 30GHz and $\epsilon_r = 3.0$

While Figure 16 is useful for those familiar with working with wavelengths, Figure 17 additionally defines a Gap-Rate Distance (GRD) in mils that can be immediately applied when placing a GRV near an SV on a PCB. To avoid problematic signal paths (IL and TDR metrics) shown elsewhere in this paper, GRD is defined to be the maximum center-to-center (c2c) distance between an SV and its closest associated GRV(s) for a given data rate, based on guard bands. GRD is derived by solving Equation (26) for distance *d*, fixing CW=0.16, and frequency *f* to two times the data rate's fundamental frequency to reasonably address the spectral content involved. CW is reduced from 0.25 to 0.16 to guard band variables and tolerances such as via hole sizes, antipads, dielectric constants, and other factors. While many GRD solutions are possible, this plot can be practically applied in many high-frequency applications to avoid adding excessive via IL to a signal path.

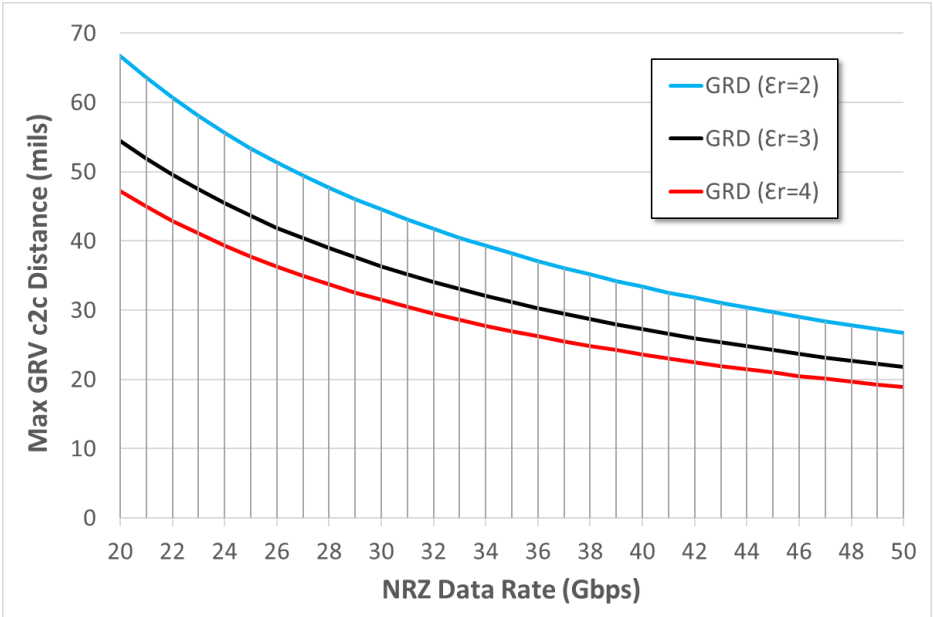

Figure 17: GRD Metric (guard bands: CW=0.16, freq=2xfundamental)

6.3 Transmission Path Discontinuities

Figure 18 shows the measured (at left, repeated from Figure 2) and calculated single ended via's TDR response for both "square" and "diamond" GRV patterns. As the mathematical model is not bandwidth-limited, calculated results are shown both at the bandwidth of the measurement (center) and out to 60 GHz (right). As shown, the increase in peak impedance for the "square" GRVs is 5 Ohms higher than the "diamond" GRVs in both measurement and simulation. However, what isn't visible in the measurement yet visible using the model (right), signals with a higher data rate and/or spectral content can be expected to see a significantly higher discontinuity. For this comparison, the stacked via cell model is used to approximate the actual via's length.

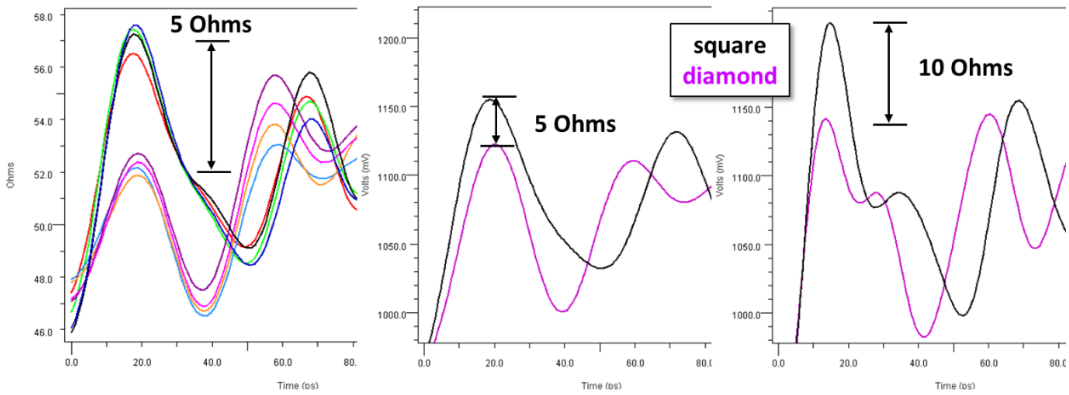

Figure 18: Single-ended TDR for stacked PCB layer model

6.4 Crosstalk

At higher frequencies interactions of via ground return currents become the primary and significant source of crosstalk. As shown in Figure 3 and repeated in Figure 19 (left), vias separated by more than 140 mil experience crosstalk greater than 20 dB above 30 GHz, again by amounts dependent GRV structures. As Figure 3's measurement includes the larger system, to illustrate that the high-frequency crosstalk is due *only to the via structures*, Figure 19 compares measured and simulated crosstalk by using *only the via models* in the simulation. While some aspects of the full system measurement, such as ripple related to trace length, are not seen in the via-only simulation, the dominant high-frequency magnitudes are clearly attributable to the signal vias and their ground return interactions. Simulation again allows a larger frequency range than achieved in measurement as shown, and also utilizes the fully stacked PCB model.

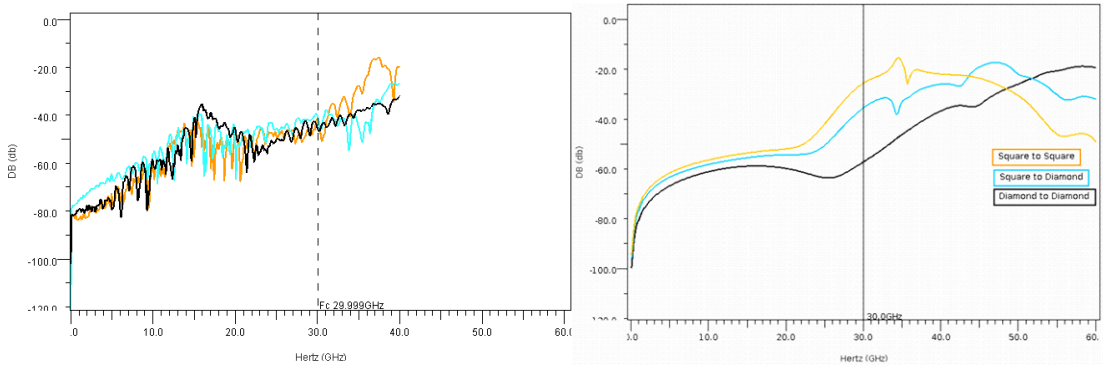

Figure 19: Measured System Crosstalk versus Via Only Crosstalk

7 Future Studies

We are actively pursuing a number of extensions to the work presented in this paper. The following sections describe some of the extensions for which we have made some progress.

7.1 Differential Vias

Although single-ended vias are used directly in some applications and they have proven to be a valuable vehicle for study, many high-speed serial channels use differential transmission, including differential vias. It is therefore imperative to study how GRVs affect IL, impedance discontinuities, and crosstalk specifically for differential transmission.

Figure 20 illustrates a layout for studying how GRVs affect the crosstalk between nearby differential vias. In this layout, the separation between the true and complement vias in a differential pair is 1 mm, and there is a single aggressor differential pair 2 mm away. The figure shows sixteen GRVs available for shielding the differential vias. Four different cases were evaluated: no shielding GRVs, only two GRVs between the differential vias, four GRVs between the differential vias, and a full set of sixteen GRVs shielding this section of the layout.

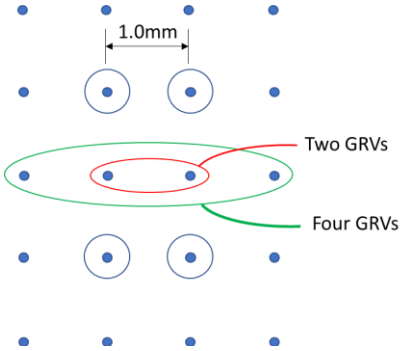

Figure 20: Layout for differential transmission crosstalk study

Figure 21 is a plot of the results for a single PCB layer. Whereas two GRVs reduce the crosstalk by a modest 5 dB compared to the no GRV case, four GRVs provide a disproportionately greater reduction.

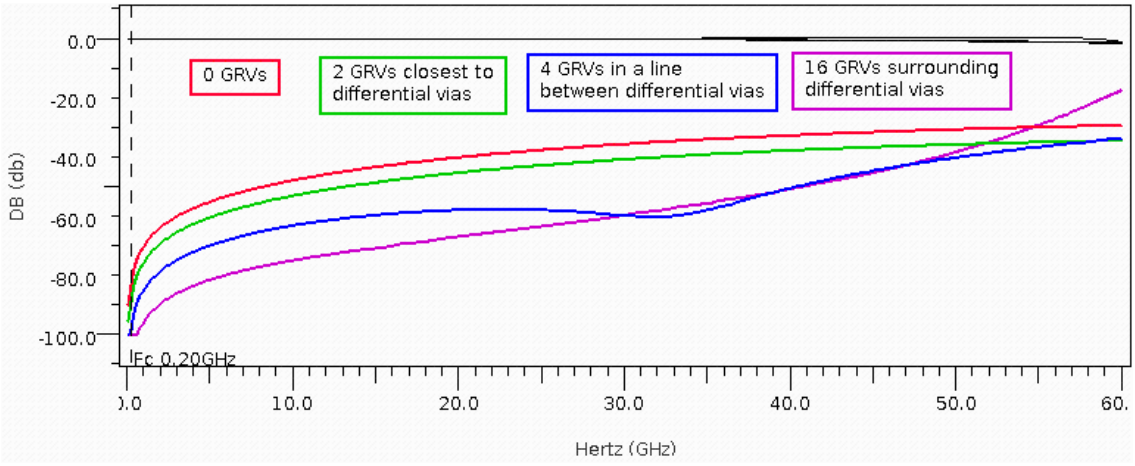

Figure 21: Differential via crosstalk as a function of number and configuration of GRVs

7.2 DC Power Planes

If signal vias pass through one or more DC power planes, that introduces an additional configuration to be analyzed, as illustrated in Figure 22. In this configuration, the GRVs are shorted to the return planes, as usual. However they must be isolated from the power plane by antipads. Because power planes typically need to be placed near the center of the PCB stackup for mechanical reasons, this configuration will occur on almost every board design.

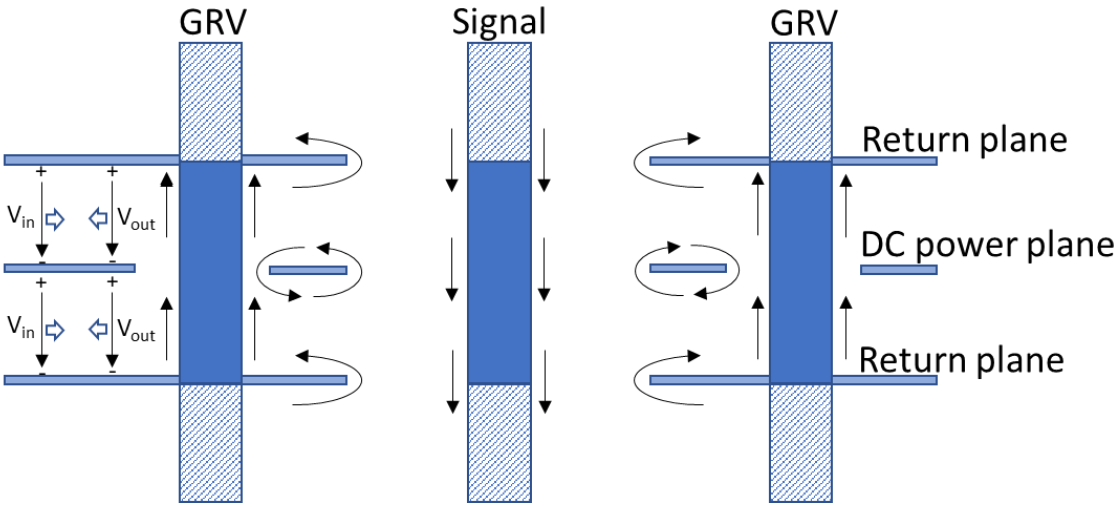

Figure 22: Signal propagation through a DC power plane

In this configuration the GRV's reflection of the fields from the signal via is more complex than it is for a GRV between two return planes:

1. The electric field from the signal's via cell propagates to the return path of the GRV, asserting an input voltage on the return path of the GRV.
2. The short circuits at the return planes apply the return path input voltage to the barrel of the GRV.
3. A current flows in the barrel of the GRV to produce a zero-order radial TEM wave with sufficient amplitude to cancel the voltage applied to the return path.
4. The radial TEM wave from the GRV barrel propagates back to the signal's via cell.

In the process of transmitting the return voltage to the GRV barrel, there will be some transmission of energy in the vertical direction, and therefore some transmission delay. The resulting delay has the same effect as if the GRV were connected to the return plane but placed a dielectric thickness further from the signal's via cell. This effect may not be particularly important if the dielectrics surrounding the power plane are relatively thin, but could become more significant if the dielectrics surrounding the power plane are thick, or multiple power planes have been stacked together without return planes between them.

7.3 Higher-Order Modes

As observed in section 4.2, the only modes that can imply a current inside a via cell are ones that are centered inside the antipad. Furthermore, the only radial TEM mode for which the integral of the magnetic field around the center is nonzero is the zero-order mode. All higher-order modes

have an angular variation that will integrate to zero around the entire circumference of the antipad.

However, modes from outside the antipad or higher order radial TEM modes centered inside the antipad can have a net current in or out over part of the circumference of the antipad, only to be canceled out by currents in another part of the circumference of the same antipad. Currents are flowing into the antipad on one side and flowing out on another.

A stricter boundary condition is that over the entire circumference of the antipad, the only surface currents perpendicular to the edge of the antipad are those that were induced by the barrel current. That would be the lowest energy solution, and therefore the condition toward which the structure would converge.

In general, there can be higher order modes centered inside an antipad to redirect current around the antipad because the current cannot flow across the antipad. Figure 23 illustrates such a situation. Relatively uniformly distributed current is flowing in from the top of the figure and out at the bottom. However, currents from a second-order mode inside the antipad are forcing the current to flow around the antipad, deflecting the current away from the antipad at the top of the antipad and drawing it back together at the bottom. Meanwhile, the net current flowing into or out of the antipad is zero – as much current is flowing in at the bottom as is flowing out at the top.

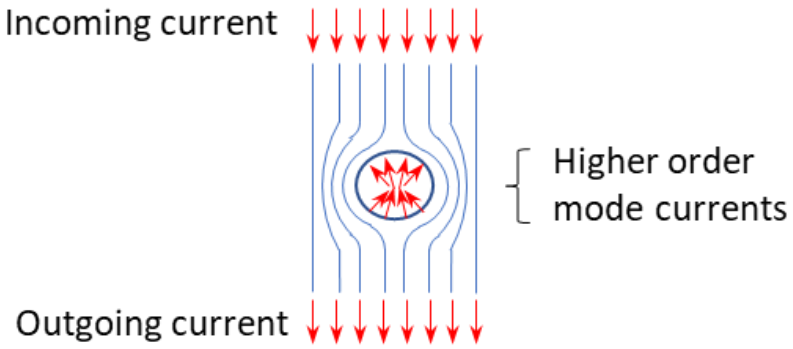

Figure 23: Higher order mode currents deflecting current around an antipad

The higher order modes decay more rapidly than the zero order mode. However, they can be important when features such as GRVs are relatively close to the edge of the antipad.

8 Conclusions

This paper presents a study of the interaction between GRVs and single-ended signal vias. We have noted that GRVs tend to interact with each other through constructive interference, with two or more GRVs forming a resonant cavity. When larger numbers of GRVs combine to form a resonant cavity, the constructive interference compounds to dramatically increase the Q of the cavity.

The higher Q has both advantages and disadvantages, depending on how close the frequencies of interest are to the resonant frequency of the cavity. Outside of the frequency range of the resonant response, the GRV cavity provides a nearly ideal return path for the via. However, within the frequency range of the resonant response, the return path can degrade quite abruptly, causing dramatically increased transmission path discontinuities and IL. As such, a GRD metric has been provided to help PCB engineers avoid this phenomenon.

We have also observed that except when vias are so close together that they can couple capacitively, the dominant crosstalk mechanism is the return path voltage induced by radial TEM waves propagating between the return planes. This crosstalk can propagate at least several wavelengths with relatively low loss. It appears that the most effective countermeasure against this form of crosstalk is a resonator of GRVs close to either the aggressor or the victim. The higher the Q of the GRV resonator, the greater the crosstalk rejection.

References

1. Donald Telian, “Signal Integrity, In Practice – A Practical Handbook for Hardware, SI, FPGA & Layout Engineers” – book published in 2022 and available at Amazon.
2. Telian, Camerlo, et al., “Simulation Techniques for 6+ Gbps Serial Links”, DesignCon 2010.
3. Steinberger, Wildes, Brock and Katz, “When Shorter Isn’t Better”, DesignCon 2010.
4. Michael Steinberger, “The Long and the Short of Eye Masks”, Signal Integrity Journal, September 19, 2021.
5. Telian, Camerlo, Steinberger, Katz and Katz, “Simulating Large Systems with Thousands of Serial Links”, technical paper, DesignCon 2012.
6. Steinberger, Brock, Telian, “Fast, efficient and accurate: via models that correlate to 20 GHz”, technical paper, DesignCon 2013.
7. Ramo, Whinnery and Van Duzer, *Fields and Waves in Communication Electronics*, third edition, John Wiley and Sons, Inc., copyright 1994.
8. Ding, Gopinath, Scearce, Steinberger and White, “A Simple Via Experiment”, technical paper, DesignCon 2009.
9. Rimolo-Donadio, Müller, Duan, Kotsev, Brüns, Schuster, “Efficient, Physics-Based Via Modeling: Principles and Methods”, IEEE Electromagnetic Compatibility Magazine, Volume 1, Quarter 1, 2012.
10. Djordjevic, Biljic, Likar-Smiljanic and Sarkar, “Wideband Frequency-Domain Characterization of FR-4 and Time-Domain Causality”, IEEE Transactions on Electromagnetic Compatibility, Vol. 43, No. 4, pg. 662-7, November 2001.
11. Horn, LaFrance, Caisse, Coonrod and Fitts, “Effect of conductor profile structure on propagation in transmission lines”, technical presentation, DesignCon 2015.
12. Koledintseva, Kashurkin, Vincent and Hinaga, “Effective Roughness Dielectric to Represent Copper Foil Roughness in Printed Circuit Boards”, technical paper, DesignCon 2015.